Analysis of adsorption of azo dye onto NiAl-CO$_3$ using Box-Behnken design approach and desirability function

K. El Hassani[1], B.H. Beakou[1], A. Anouar[1*]

[1] *Laboratory of Applied Chemistry and Environment, Faculty of Science and Technology of Settat, Hassan first University, Settat, Morocco.*

Abstract
Batch adsorption process was used for Methyl Orange (MO) azo dye removal from aqueous solution onto flower-like Ni-Layered Double Hydroxide adsorbent, prepared in our previous work. The weights of the effects of the change of initial dye concentration (C$_0$: 100–500 mg/L), temperature (T: 10–50 °C) and adsorbent dose (w: 0.33–1 g/L) on removal efficiency (%) were evaluated. The response surface methodology (RSM) based on 3-variable 3-level Box–Behnken design was applied. The effects of the experimental factors on the removal efficiency of MO from aqueous medium onto adsorbent fitted the adopted polynomial model, and the weights of the effects of the factors followed the order: initial dye concentration > temperature > dose. The effects of the interactions between the factors on the adsorption properties were evaluated and discussed in relation to the mechanism of elimination.

1. Introduction

Azo dyes and their pigments are the largest chemical groups of dyes in existence constituting 60–70% of all industrial dyestuff production [1,2], which make them the most common synthetic colorants released into the environment [3]. Thus, several studies were focusing on resolving this issue adopting various wastewater treatment technologies such as advanced oxidation processes (AOP) [4], photocatalysis [5], chemical oxidation [6], membrane technique [7] and biological processes [8].

The adsorption process represents the common technique for wastewater treatment and removal of organic pollutants compared to other conventional processes [9–15]. However, the adsorption capacity of the adsorbents depend on different factors such as temperature, adsorbent dose, contact time, initial adsorbate concentration, particle size, pH of solution, etc … [16–19]. Hence, the investigation of the evolution of a chemical property of the adsorbent's adsorption capacity as a function of all the operating factors required several experiments.

The response surface methodology (RSM), as a powerful statistical based technique, is employed to optimize and/or minimize the number of experiments, it facilitates the anticipation of the effect of simultaneous variations of factors, and thus searching for the optimum operational conditions for the system that satisfies the operating specifications [20,21]. RSM can be used to predict the response of a system via a mathematical model at any new operating conditions.

In this study, the removal of MO dye was carried out by adsorption process using Ni-based layered double hydroxides (LDHs) materials. LDHs are a class of synthetic two dimensional nano-structured inorganic materials [22]. The unique properties of LDHs make them used in many applications, especially in wastewater treatment systems [23–28]. Mahjoubi et al. [29] have investigated the adsorption capacity of MO dye onto different LDH phases (Zn-, Mg- and Ni-based LDH). The results indicate that the obtained LDH phases are promising precursors for the treatment of the actual dye from textile wastewater. Thus, they are regarded as strong adsorbents for dyes removal from aqueous solution [30–32]. The use of these materials were also reported in our previous work [33], where we focused on removing MO dye using low-cost and efficient adsorbing materials. Two adsorbents with different morphologies were synthetized. Interestingly, unlike conventional Ni-LDH adsorbent, Ni-LDH with flower-like morphology exhibits an excellent adsorption capacity for MO removal from aqueous solution.

Therefore, in this work, the combined effect of three operating factors (adsorbent dose, initial dye concentration and temperature) on MO removal from aqueous medium by f-NiAl adsorbent was studied using an experimental design. The Box-Behnken design coupled with desirability function (DF) was applied to achieve the optimum levels of the effective factors using Design Expert version 100.0.0 (Stat Ease) Software.

2. Material and Methods
2.1. Adsorbent and adsorbate
Methyl orange (MO) dye was purchased from Sigma-Aldrich and was used as received without further purification. The stock dye solution (1000 mg/l) was prepared by dissolving an accurate amount of dye in the distilled water. Experimental solutions of the desired concentrations were obtained by successive dilutions with distilled water. Ni-based LDH adsorbent, noted as f-NiAl, was prepared according to our previous study [27].

2.2. Experimental program
For each experimental run, 30 mL of MO solution of 100, 250 or 400 mg/L initial concentrations (C_0) at a fixed pH and for known contact time of 4 hours were taken in a 100 mL in jacketed beaker. Initial pH of the adsorbate solution was adjusted at 3 by the addition of 0.1N or 1N aqueous solutions of HNO_3 (Sigma-Aldrich, 90%). This mixture was agitated at a constant speed of 150 rpm at different temperatures (T: 10, 30 or 50 °C), with the addition of a known dose of the adsorbent (w: 0.33, 0.665 or 1 g/L). All the samples were centrifuged at 7000 rpm for 5 min (Sigma 2-15 centrifuge) and analyzed for the residual dye concentration using a UV–vis spectrophotometer (Hach DR6000™). The MO dye removal rate (Y) by Ni-LDH adsorbent was calculated as:

$$Y(\%) = [\,(C_0 - C_e)/C_0\,].\,100\% \qquad (1)$$

C_0 is the initial adsorbate concentration (mg/L), C_e is the adsorbate concentration (mg/L) at equilibrium time.

2.3. Modelling and design of experiments
The 3-factor 3-level Box-Behnken experimental design was applied to study the operational variables affecting the removal process of MO dye using f-NiAl adsorbent. Initial dye concentration (C_i: 100-400 mg/L), temperature (T: 10–50 °C), and adsorbent dose (w: 0.33-1 g/L) are variable input parameters, while contact time (4 hours) and pH of solution (~3) were kept as constant input parameters. The factor levels were coded as +1 (high), 0 (central point) and -1 (low) [34]. Table 1 shows the variables and levels of the Box-Behnken design model.

Table 1: Experimental design levels of chosen variables.

Parameters	Unit	Range and level		
		-1	0	+1
Factors				
x_1 : Initial OM concentration (Ci)	mg/L	100	250	400
x_2 : Temperature (T)	°C	10	30	50
x_3 : adsorbent dose (w)	g/L	0.33	0.665	1
Response				
Y : Removal efficiency	%			

The removal efficiency of MO dye (Y) is selected as a response for the combination of independent variables, which is fitted by a second order polynomial model:

$$Y = a_0 + \sum_{i=1}^{n} a_1 x_i^2 + \sum_{i=1}^{n} a_{ii} x_i^2 + \sum_{i=1}^{n-1} \sum_{j=1}^{n} a_{ij} x_i x_j + e \quad (2)$$

Where Y is the predicted response value associated with each factor level combination; a_0 is constant; and a_i, a_{ii}, and a_{ij} are linear effect, quadratic effect, and 2-way linear by linear interaction effect, respectively; x_i and x_j are the coded values of independent variables; and e is the residual error [35].

3. Results and discussion
3.1. Box–Behnken design and regression model
The optimization using the Box-Behnken design requires 15 experiments for modeling a response. This number of experiments has been performed to evaluate the effects of the three main independent parameters (initial concentration of the dye, Temperature, and adsorbent dose) on the MO removal efficiency Y (%). Box–Behnken

design matrix for real and coded values along with experimental and predicted values for removal efficiency (%) of MO by f- NiAl adsorbent is shown in Table 2. The maximum dye removal efficiency (%) was found to be 99.89% (Table 2).

Table2: Experimental and predicted values of Removal efficiency for MO adsorption onto f-NiAl

Run order	Coded (real) values			Removal efficiency (%)	
	x_1	x_2	x_3	Experimental	Predicted
1	-1 (100)	-1 (10)	0 (0,665)	99.89	100.23
2	+1 (400)	-1 (10)	0 (0,665)	96.65	96.06
3	-1 (100)	+1 (50)	0 (0,665)	98.57	99.16
4	+1 (400)	+1 (50)	0 (0,665)	65.41	65.06
5	-1 (100)	0 (30)	-1 (0,33)	97.01	96.31
6	+1 (400)	0 (30)	-1 (0,33)	66.48	66.71
7	-1 (100)	0 (30)	+1 (1)	98.19	97.96
8	+1 (400)	0 (30)	+1 (1)	88.58	89.29
9	0 (250)	-1 (10)	-1 (0,33)	93.48	93.84
10	0 (250)	+1 (50)	-1 (0,33)	69.68	69.80
11	0 (250)	-1 (10)	+1 (1)	98.06	97.95
12	0 (250)	+1 (50)	+1 (1)	90.28	89.92
13	0 (250)	0 (30)	0 (0,665)	95.68	95.86
14	0 (250)	0 (30)	0 (0,665)	96.14	95.86
15	0 (250)	0 (30)	0 (0,665)	95.76	95.86

3.2. Model adequacy checking

Linear, interactive (2FI), quadratic and cubic models were fitted to the experimental data to obtain the regression models. The adequacy of the generated models was analyzed by the analysis of variance, lack-of-fit tests and correlation coefficient. The results are shown in Table 3. From the adequacy of model summary, the quadratic model was found to be the most suitable among the four studied models. The correlation coefficient of quadratic model was higher comparing to other models. The probability less than 0.100 indicates that the model is highly significant [36]. The lack of fit p-value was greater than 0.05 (P-value = 0.074), where a non-significant lack-of-fit confirms that quadratic model was valid for the adsorption MO onto f-NiAl adsorbent.

Table 3: Adequacy of the models tested

Source	Sequential p-value	Lack of fit p-value	Adjusted R^2	Predicted R^2	Standard divisions	
Linear	0.0015	0.001	0.6675	0.4898	7.04	
2FI	0.0116	0.0025	0.8765	0.8313	4.29	
Quadratic	<0.0001	0.074	0.9967	0.9821	0.70	Suggested
Cubic	0.0774		0.9996		0.25	Aliased

3.3. Statistical analysis

An empirical relationship represented by a second-order quadratic equation in terms of coded factors was used to predict the maximum removal efficiency of MO. The final equation obtained is given in Table 4.

Table 4: Analysis of variance (ANOVA) results for response parameters

Modified equation with significant terms	R^2	Adjusted R^2	Predicted R^2	Adequate precision	SD[a]	CV[b]	PRESS[c]
R (%)= $95.86 - 9.57x_1 - 8.02x_2 + 6.06x_3 - 3.02x_1^2 - 2.71x_2^2 - 5.27x_3^2 - 7.48x_1x_2 + 5.23x_1x_3 + 4.01x_2x_3$ (3)	0.998	0.996	0.9821	61.782	0.7	0.77	37.22

[a] Standard deviation; [b] Coefficient of variation; [c] Predicted residual error sum of squares.

By checking the normal probability plot of the residuals (Figure1), the normality of residuals and the adequacy of the model can be verified. As shown in Figure 1a, the data values fit almost near to a fairly straight line, indicating that the errors are normally distributed and the model is adequate. The plot of the experimental versus predicted values based on Eq. (3) was illustrated in Figure 1b. The square of the correlation coefficient value (R^2) was 0.9988, indicating that 0.12% of the total variations could not be explained based on the predicted model. The Predicted R^2 of 0.9821 is in reasonable agreement with the Adjusted R^2 of 0.9967 (i.e. the difference is less than 0.2). The Adjusted R^2 value is close to 1.0, suggesting that the model (Eq. (3)) has high reliability for predicting the corresponding experimental data.

The "Adequate precision" measures the signal to noise ratio. A ratio greater than 4 is desirable. In our study, the value indicates an adequate signal. The model can be used to navigate the design space.

F-value and p-value can also evaluate the significance of the model coefficients. As seen from Table 5, all the linear and their interactive terms were found to be statistically significant ($p < 0.05$). The large F-value of 475.98 indicates that most of the variation in the response can be explained by the regression equation.
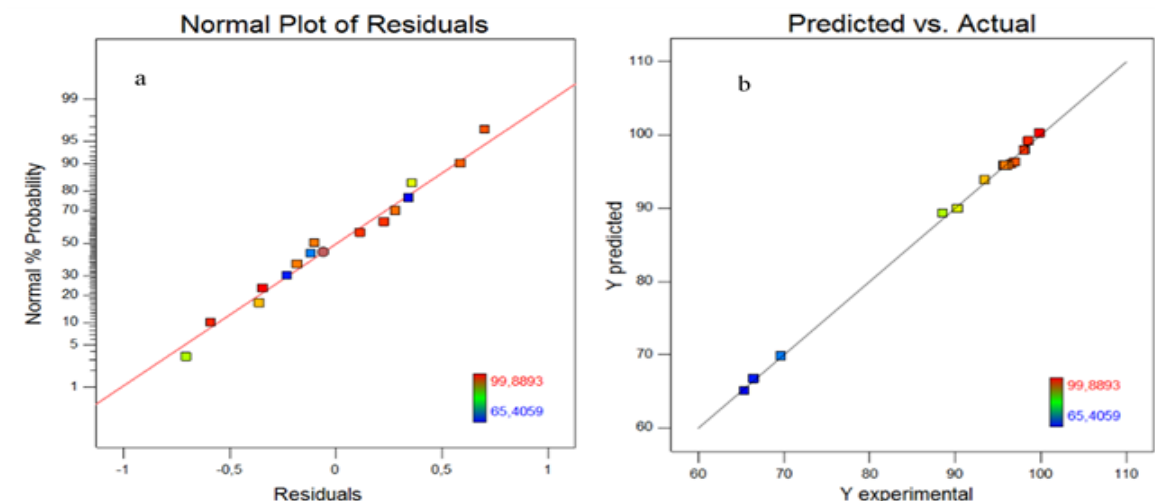

Figure 1: (a) Normal plot of Residuals and (b) Scatter plot of predicted response versus experimental response for MO removal

Table 5: Analysis of variance (ANOVA) of the fitted quadratic model

Source	Degrees of freedom	Sum of squares	Mean squares	F-value	p-Value (F $> F_{0.05}$)	Remarks
Regression	9	2082.42	231.38	475.98	<0.0001	Highly significant
x_1	1	732.40	732.40	1506.64	<0.0001	
x_2	1	514.21	514.21	1057.79	<0.0001	
x_3	1	293.62	293.62	604.01	<0.0001	
x_1^2	1	33.65	33.65	69.21	0.0004	
x_2^2	1	27.11	27.11	55.76	0.0007	
x_3^2	1	102.60	102.60	211.06	<0.0001	
x_1x_2	1	223.89	223.89	460.58	<0.0001	
x_1x_3	1	109.42	109.42	225.10	<0.0001	
x_2x_3	1	64.18	64.18	132.02	<0.0001	
Residual error	5	2.43	0.49			
Lack of fit	3	2.31	0.77	12.67	0.074	Not significant
Pure error	2	0.12	0.061			
Total	14	2084.85				

3.4. Effects of process variables

To visualize the effect of the three independent factors and their interactions on the MO removal rate, the three-dimensional response surface diagrams based on the predictive quadratic model (Eq. (3)) for the MO removal efficiency were shown in Figure 2a, b, c.

The effect of temperature was remarkable for the removal of MO by f-NiAl (Figure 2a-c). At any particular w or C_i, MO removal decreased with an increase in T from 10-50 °C. At an initial concentration of C_i = 400 mg/L and adsorbent dose of w = 0.665 g/L, the removal efficiency of MO dye decreased from 96.65 % to 65.41 %

with an increase in temperature from 10 °C to 50 °C. This indicates that the adsorption mechanism is an exothermic process in nature [37]. This might occur because of the tendency of organic molecules to escape from the solid phase of f-NiAl adsorbent to the aqueous phase of MO dye with an increase in temperature [38].
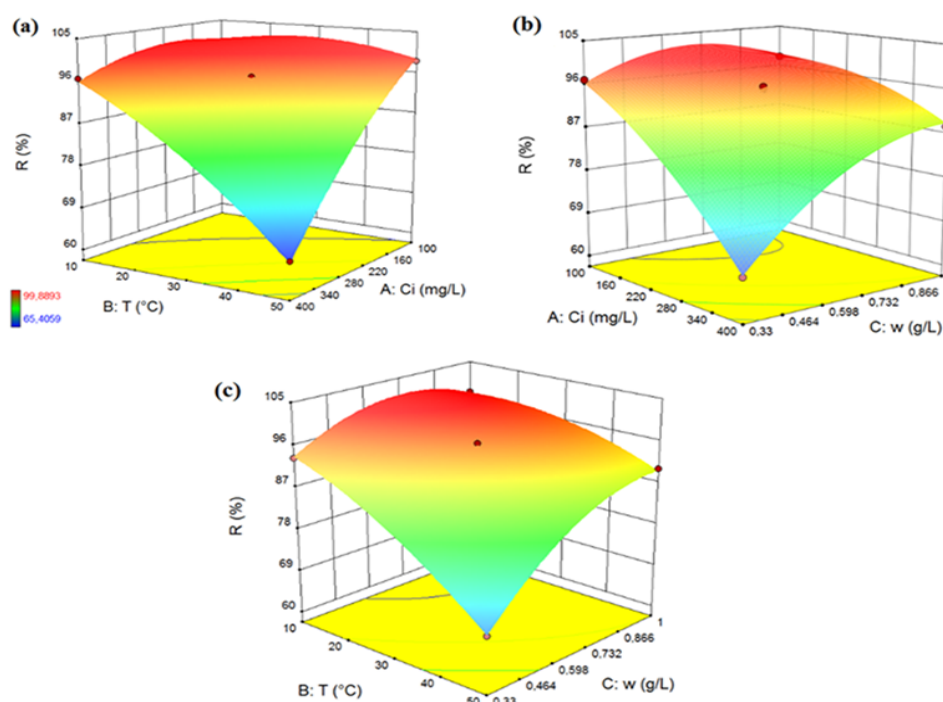

Figure 2: Response surface diagram: (a) effect of C_i and T on MO removal at adsorbent dose 0.665 g. L^{-1}; (b) effect of w and C_i on MO removal at temperature 30 °C; (c) effect of w and T on MO removal at initial concentration 250C mg/L.

Indeed, the thermodynamic behavior of MO molecules adsorption onto f-NiAl was investigated by estimating the thermodynamic parameters (Gibbs free energy change ΔG° [kJ/mol], standard enthalpy change ΔH° [kJ/mol], and the standard entropy change ΔS° [J/mol·K]), which can determine whether the adsorption process is spontaneous or not, and endothermic or exothermic.

The ΔG° value at a selected temperature can be obtained from the following thermodynamic equation:

$$\Delta G^{\circ} = -RT ln K_c \quad (4)$$

Where, R is the universal gas constant (8.314 J.mol^{-1}K^{-1}), and T is the absolute temperature (K) and K_c is the single point or linear adsorption distribution coefficient defined as [39,40]:

$$K_c = \frac{Q_e}{C_e} \quad (5)$$

Besides, the values of ΔH° and ΔS° can be estimated from the following thermodynamic equation:

$$ln K_c = -\frac{\Delta H^{\circ}}{RT} + \frac{\Delta S^{\circ}}{R} \quad (6)$$

Note that the slope and ordinate of a linear plot of lnK_c versus $1/T$ correspond to the ΔH°/R and ΔS°/R, respectively. The linear plot is presented in Figure 3.

The resulting thermodynamic parameters values are presented in Table 6. The negative values of ΔG° indicated that the removal process was spontaneous. Also, the increase in the negative value of ΔG° with an increase in temperature confirms that the removal process is advantageous at lower temperatures. Note that the value of K_c decreased with temperature and a negative value of ΔH° confirms that the adsorption phenomenon was exothermic in nature. Further, a negative entropy change (ΔS°) indicates that the removal process is enthalpy driven. It also suggests a decreased randomness at the adsorbent/dye solution interface during the adsorption process leading to the escape of the adsorbate molecules from the solid phase to the liquid medium; which explain the decrease of removal efficiency with increasing temperature of the solution. The adsorption of MO onto f-NiAl was performed at different initial dye concentrations in the range of 100–400 mg/L. According to Figure 2a-b, it was clearly noticeable that the removal rate of MO dye decreased with increasing the initial concentration. Yet, the adsorption capacity of MO dye increased due to a rise in interactions between f-NiAl adsorbent and MO dye molecules [41]. Indeed, during adsorption, the initial concentration of organic molecules can provide an important driving force to overcome all mass transfer resistances between the dye and adsorbent

phase [10,42]. Also, at a given adsorbent dosage, lower removal efficiency was observed due to the low availability of more adsorption sites at higher initial dye concentration, and the adsorption of MO dye will rely on its initial concentration.
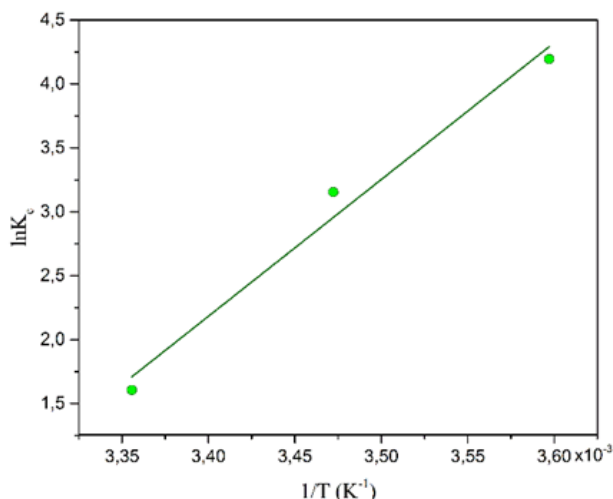

Figure 3: Linear plot of lnK_c versus 1/T.

Table 6: Values of thermodynamic parameters for MO removal by f-NiAl.

T (°C)	K_c	$-\Delta H°$ (KJ/mol)	$-\Delta S°$ (J/K.mol)	R^2	$-\Delta G°$ (KJ/mol)	Y (%)
5	66.37				9.92	98.95
15	23.46	88.92	284.1	0.982	7.07	95.91
25	4.98				4.23	83.29

The adsorbent dose is another impactful parameter in the adsorption process, which determines the potential of adsorbent to remove the pollutant species at a given initial concentration [43,44]. From Figure 2b-c, generally, the removal efficiency increased with an increase in the adsorbent dose from 0.33 g/L to 1 g/L. Hence, increasing the adsorbent dose provided greater surface area and more dye binding sites.

3.5. Independent variables
The individual effect of three factors was also studied using perturbation plot for the removal of MO dye. The perturbation plot was used to compare the effect of three factors simultaneously at the center point in the design space and was shown in Figure 4. The plot does not show the effect of interactions and it is like one factor at a time experimentation.
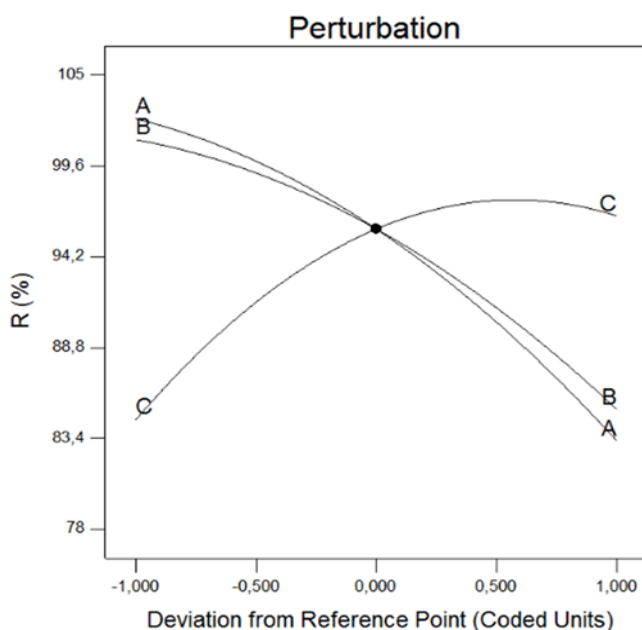

Figure 4: Plot of perturbation of all three factors.

The response was obtained by varying only one factor over its range while holding the other factors constant. A steep slope or curvature in the resulting plot indicates that the response is sensitive to that factor. In this case, at the center point, factor A (initial concentration) produces a relatively high effect on dye removal. Factor B (temperature) has the same effect as factor A. The effect of factor C (adsorbent dose) is the inverse of both terms mentioned.

3.6. Optimization using the desirability function

The profile for desirable option with predicted values was used for optimization of the removal process. The desired goal properties were identified by adjusting the weight or the importance that might alter the properties of a goal. Where, the level of temperature of colored solution within range of 10–50 °C, a maximum level of initial dye concentration (400 mg/L), minimum level of f-NiAl adsorbent dose (0.33 g/L), and maximum level dye removal, were set for maximum desirability.

In Figure 5, the optimal variable settings for the maximum dye removal based on DF methodology are achieved at initial concentration of 399.9 mg/L, 0.44 g/ of adsorbent dose, low temperature of 10 °C, dye removal of 88.99 % and desirability of 0.828. For validation, the experiments were done in duplicate using the optimized parameters. Comparing with the optimized data obtained using desirability function, similar results were obtained. Finally, the Box–Behnken design combined with desirability functions could be effectively used to optimize the adsorption parameters for the removal of MO dye by f-NiAl adsorbent.
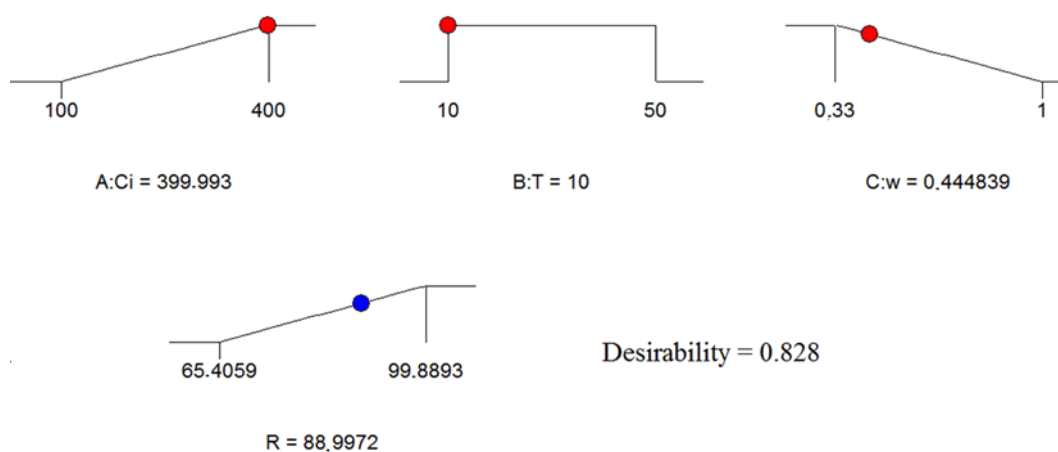

Figure 5: Desirability ramp for numerical optimization of three selected goals.

Conclusion

In this study, Box–Behnken design was applied to evaluate the effects of three process factors on MO dye removal by f-NiAl adsorbent. The significant and robustness of the quadratic model was confirmed by ANOVA analysis. The second-order polynomial regression model has also been found to properly describe the experimental data with coefficient of determination (R^2) value of 0.998 and an F-value of 475.98. The adsorption of MO onto f-NiAl was found to be exothermic in nature. Based on the desirability function, the optimized conditions were at initial concentration of 399.9 mg/L, 0.44 g/ of adsorbent dose, temperature of 10 °C for a desirability of 0.828. Hence, the Box–Behnken model is suitable to optimize the experiments for MO removal onto f-NiAl adsorbent.

References

1. C. Carliell, S. Barclay, N. Naidoo, C. Buckley, D. Mulholland, *E. Senior, Water (SA)*. 21 (1995) 61.
2. I.K. Konstantinou, T.A. Albanis, *Appl. Catal. B Environ*. 49 (2004) 1–14.
3. K. Selvam, K. Swaminathan, K.-S. Chae, *Bioresour. Technol*. 88 (2003) 115–119.
4. H. Song, J.-A. You, C. Chen, H. Zhang, X.Z. Ji, C. Li, Y. Yang, N. Xu, J. Huang, *J. Environ. Chem. Eng*. 4 (2016).
5. S. Sabar, M.A. Nawi, W.S.W. Ngah, *Desalin. Water Treat*. 57 (2016) 5851–5857.
6. C. Jung, Y. Deng, R. Zhao, K. Torrens, *Water Res*. 108 (2017) 260–270.
7. L. Yao, L. Zhang, R. Wang, S. Chou, Z. Dong, *J. Hazard. Mater*. 301 (2016) 462–470.
8. M. Punzi, A. Anbalagan, R. Aragão Börner, B.-M. Svensson, M. Jonstrup, B. Mattiasson, Chem. Eng. J. 270 (2015) 290–299.

9.   R. Qadeer, *Colloids Surfaces A Physicochem. Eng. Asp.* 293 (2007) 217–223.
10. T.W. Seow, C.K. Lim, *Int. J. Appl. Eng. Res.* ISSN. 11 (2016) 973–4562.
11. K. Liu, L. Chen, L. Huang, Y. Lai, *Carbohydr. Polym.* 151 (2016) 1115–1119.
12. Y. Tang, Q. Zhou, Y. Zeng, Y. Peng, *J. Dispers. Sci. Technol.* 38 (2017) 347–354.
13. S.E. Subramani, N. Thinakaran, Isotherm, *Process Saf. Environ. Prot.* 106 (2017) 1–10.
14. B.H. Beakou, K. El Hassani, M.A. Houssaini, M. Belbahloul, E. Oukani, A. Anouar, *Water Sci. Technol.* 76 (2017) 1447–1456.
15. B.H. Beakou, K. El Hassani, M.A. Houssaini, M. Belbahloul, E. Oukani, A. Anouar, *Sustain. Environ. Res.* 27 (2017) 215–222.
16. R.M.M. dos Santos, R.G.L. Gonçalves, V.R.L. Constantino, C.V. Santilli, P.D. Borges, J. Tronto, F.G. Pinto, *Appl. Clay Sci.* 140 (2017) 132–139.
17. D.A. Giannakoudakis, G.Z. Kyzas, A. Avranas, N.K. Lazaridis, *J. Mol. Liq.* 213 (2016) 381–389.
18. E. Daneshvar, A. Vazirzadeh, A. Niazi, M. Kousha, M. Naushad, A. Bhatnagar, *J. Clean. Prod.* 152 (2017) 443–453.
19. F.P. De Sá, B.N. Cunha, L.M. Nunes, *Chem. Eng. J.* 215–216 (2013) 122–127.
20. R.H. Myers, D.C. Montgomery, C.M. Anderson-Cook, Response Surface Methodology: Process and Product Optimization Using Designed Experiments, 3rd Edition, y John Wiley & Sons, Inc., New Jersey, 2015.
21. D.C. Montgomery, Design and Analysis of Experiments, 8th ed., John Wiley & Sons, Inc., 2012.
22. S. Miyata, *Clays Clay Miner.* 31 (1983) 305–311.
23. Y. Lu, B. Jiang, L. Fang, F. Ling, J. Gao, F. Wu, X. Zhang, *Chemosphere.* 152 (2016) 415–422.
24. G. Sheng, J. Hu, H. Li, J. Li, Y. Huang, *Chemosphere.* 148 (2016) 227–232.
25. B. Hudcová, V. Veselská, J. Filip, S. Číhalová, M. Komárek, *Chemosphere.* 168 (2017) 539–548.
26. H. Hur, R.J. Reeder, *J. Environ. Sci.* (2017).
27. P. Huang, J. Liu, F. Wei, Y. Zhu, X. Wang, C. Cao, W. Song, *Mater. Chem. Front.* (2017).
28. C. Lei, X. Zhu, B. Zhu, C. Jiang, Y. Le, J. Yu, *J. Hazard. Mater.* 321 (2017) 801–811.
29. F.Z. Mahjoubi, A. Khalidi, O. Cherkaoui, R. Elmoubarki, M. Abdennouri, N. Barka, *J. Water Reuse Desalin.* 7 (2017) 307–318.
30. F.Z. Mahjoubi, A. Khalidi, M. Abdennouri, N. Barka, *Desalin. Water Treat.* 57 (2016) 21564–21576.
31. R. Elmoubarki, F.Z. Mahjoubi, A. Elhalil, H. Tounsadi, M. Abdennouri, M. Sadiq, S. Qourzal, A. Zouhri, N. Barka, *J. Mater. Res. Technol.* 6 (2017) 271-283.
32. F.Z. Mahjoubi, A. Khalidi, M. Abdennouri, M., N. Barka, *J. Taibah Univ. Sci.* 11 (2017) 90–100
33. K. El Hassani, B.H. Beakou, D. Kalnina, E. Oukani, A. Anouar, *Appl. Clay Sci.* 140 (2017) 124–131.
34. M. Evans, Optimisation of manufacturing processes : a response surface approach, Carlton House Terrace, London, 2003.
35. K.Y. Benyounis, A.G. Olabi, M.S.J. Hashmi, *J. Mater. Process. Technol.* 164–165 (2005) 978–985.
36. A. Srinivasan, T. Viraraghavan, *J. Hazard. Mater.* 175 (2010) 695–702.
37. M.N. Ahmed, R.N. Ram, *Environ. Pollut.* 77 (1992) 79–86.
38. P. Saha, S. Chowdhury, Insight Into Adsorption Thermodynamics, in: M. Tadashi (Ed.), Thermodynamics, InTech, London, 2011: p. 320.
39. J.W. Biggar, M.W. Cheung, *Soil Sci. Soc. Am. J.* 37 (1973) 863.
40. A.A. Khan, R.P. Singh, *Colloids and Surfaces.* 24 (1987) 33–42.
41. R. Ahmad, *J. Hazard. Mater.* 171 (2009) 767–773.
42. M. Doğan, M. Alkan, Ö. Demirbaş, Y. Özdemir, C. Özmetin, *Chem. Eng. J.* 124 (2006) 89–101.
43. S. Kara, C. Aydiner, E. Demirbas, M. Kobya, N. Dizge, *Desalination.* 212 (2007) 282–293.
44. S. Eris, S. Azizian, *Sep. Purif. Technol.* 179 (2017) 304–308.

(2018) ; http://www.jmaterenvironsci.com